An AlGaN/GaN Based UV Photodetector Simulation Using COMSOL to Obtain the Fresnel Coefficients

Balaadithya Uppalapati[1], Akash Kota[2], Vamsy P. Chodavarapu[2], Goutam Koley[1]

[1]Department of Electrical & Computer Engineering, Clemson University, Clemson, SC, USA
[2]Department of Electrical & Computer Engineering, University of Dayton, Dayton, OH, USA
buppala@clemson.edu, kotaa1@udayton.edu, vchodavarapu1@udayton.edu, gkoley@clemson.edu

Abstract

In this paper, a novel GaN-$Al_xGa_{1-x}N$-GaN vertically stacked cantilever has been proposed to function as an ultraviolet (UV) photodetector. The proposed cantilever has been modeled in COMSOL to compute the Fresnel coefficients such as absorptance, reflectance, and transmittance in the wavelength range of 300 nm to 500 nm. Using the wave optics module, the Fresnel coefficients are computed in the given wavelength range. Simulations are performed for two different cases. In the first case, the effect of bottom GaN layer thickness variation on the Fresnel coefficients of the cantilever has been studied. The thickness of the bottom GaN layer is varied from 0.1 to 1 µm with a step size of 0.1 µm. In the second case, the effect of Al alloy composition in $Al_xGa_{1-x}N$ on the Fresnel coefficients has been studied. The Al% in $Al_xGa_{1-x}N$ has been varied from 19% to 78.5%.

Keywords: ultraviolet, photodetector, Fresnel coefficients, cantilever, AlGaN/GaN

Introduction

In the past few years, tremendous research has been carried out on the III-nitride semiconductors due to their interesting properties such as wide bandgap, high breakdown voltages, excellent mechanical and chemical stabilities, and low reverse leakage currents. Gallium nitride (GaN) and aluminum gallium nitride ($Al_xGa_{1-x}N$) are some of the examples of III-nitride semiconductors. As both GaN and $Al_xGa_{1-x}N$ are direct bandgap semiconductor materials, they are used in designing various optoelectronic devices such as light emitting diodes [1], laser diodes [2], high electron mobility transistors for sensing applications [3-5], solar cells, photodetectors [6], Schottky diodes [7].

$Al_xGa_{1-x}N$ based ultraviolet (UV) photodetectors (PDs) have attracted considerable attention in recent years because of their potential applications across various fields including military, medicine, environmental monitoring and deep space explorations. Some of the other applications of UV-PDs include solar-blind PDs [8], flame detection, missile plume sensing, covert communications, and fluorescence-based biochemical sensing [9]. Conventionally, UV-PDs are realized using photomultiplier tubes (PMTs). PMT based UV-PDs offer high sensitivity and low dark currents. PMTs are very effective for the detection of low intensity signals. But they suffer from high voltage requirements (typically $>$ 1kV), huge device volumes and fragility. An alternative approach uses UV-enhanced silicon detectors that are typically p-i-n diodes with a special anti-reflection coating designed for UV wavelength range. These semiconductor-based UV-PDs are highly reliable, robust and they can be well integrated with other semiconductor components. Although silicon UV detectors have many advantages, their dark currents are high (typically in the nA range) and quantum efficiencies are poor. Both PMT and silicon UV PDs are sensitive throughout the UV and visible wavelengths. However, they require complicated spectral filters to achieve solar-blind or visible blind operations. Ideally a UV-PD should have the sensitivity of a PMT and the robustness of a silicon detector. To realize such an ideal UV-PD, wide bandgap III-nitride semiconductor materials such as GaN and $Al_xGa_{1-x}N$ are typically used. It is because of the wide bandgap; the absorption coefficient of III-nitride materials is high in the UV region which makes them suitable for developing high performance UV-PDs. In addition, III-nitride based UV-PDs offer low dark currents and high quantum efficiencies.

For designing a typical UV PD, so far there are four types of device structures that are widely investigated in the literature. They are Schottky barrier type [10, 11], metal-semiconductor-metal (MSM) type [12-15], p-i-n type [16-18], and avalanche type [19-21]. Each of these device types are realized by using either GaN or $Al_xGa_{1-x}N$. The first Schottky barrier detector has been realized using a Ti/Au Schottky contact to p-GaN doped with Mg. The detector has absorbing electrodes on the top surface and it is illuminated from the bottom sapphire substrate [22]. MSM type PD is a variation of Schottky barrier detector. MSM PDs realized using $Al_xGa_{1-x}N$ can not operate at 0 V bias, which increases noise. But MSM PDs offer high speed of operation. $Al_xGa_{1-x}N$ based MSM PDs have also been reported with quantum efficiencies up to 47% at 262 nm [23]. P-n junction-based PDs have the advantage of low bias voltage and low dark currents due to large hetero barriers. However, the major disadvantages of p-i-n detectors are related to the difficulties in the p-type doping of GaN, and $Al_xGa_{1-x}N$ layers with high Al content. Among the p-n $Al_xGa_{1-x}N$ based PDs, the reported highest external quantum efficiency is 89% [24]. Avalanche PDs (APDs) potentially offer high internal gain via avalanche multiplication. But the realization of avalanche detectors is challenging due to issues related to nonuniform breakdown via material defects. Nevertheless, at present GaN based avalanche detectors can achieve gains as high as 10^5 to 10^6 and responsivities as high as 1 A/W. Unlike the GaN based APDs, the development of $Al_xGa_{1-x}N$ based APDs is progressing slowly because of the challenges involved in growing the high quality $Al_xGa_{1-x}N$.

In this paper, a novel GaN-$Al_xGa_{1-x}N$-GaN vertically stacked cantilever has been proposed to function as a UV PD. The focus of this paper is to study the effect of GaN thickness variation and Al alloy composition in $Al_xGa_{1-x}N$ on the Fresnel coefficients of the cantilever.

Model Geometry

The 3D geometry of the vertically stacked GaN-$Al_xGa_{1-x}N$-GaN cantilever is shown in Fig. 1(a). The thicknesses of the top GaN, intermediate $Al_xGa_{1-x}N$, and bottom GaN layers are 3 nm, 20 nm, and 1 µm respectively. Instead of simulating the entire 3D geometry, a simplified 2D geometry has been used in the finite element model. The longitudinal cross-section at the tip region of the cantilever which is shown in Fig. 1(b) is chosen for simulation. In Fig. 1(b) the width of the bottom GaN layer is 1 um. Similarly, the width of intermediate $Al_xGa_{1-x}N$ and top GaN layer is 3 um. The gap between the two adjacent $Al_xGa_{1-x}N$ layers is also 3 um. During the experiments the cantilever is surrounded by the air medium. Therefore, for the simulation purpose an air medium of 50 nm thickness is added throughout the width of the cantilever (see Fig. 1(b)).

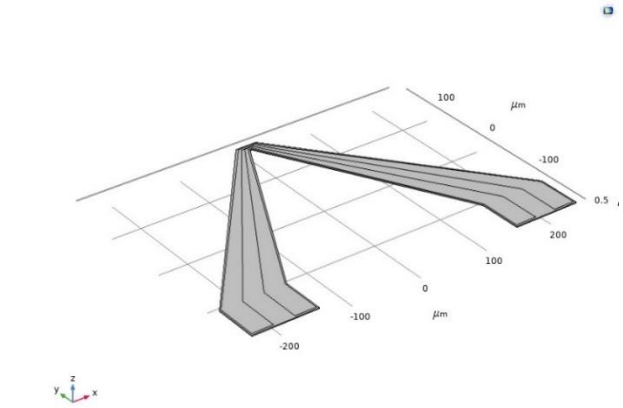

(a)

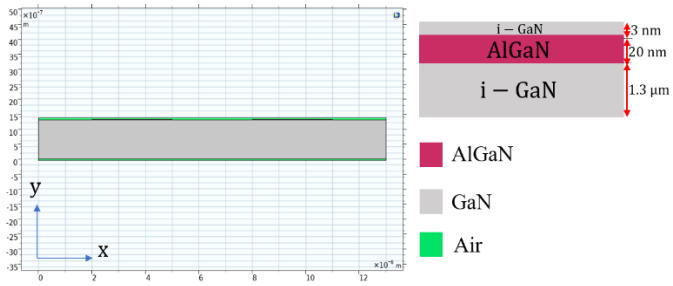

(b)

Fig. 1. (a) 3D Geometry of the GaN-$Al_xGa_{1-x}N$-GaN ultraviolet photodetector, **(b)** Longitudinal cross section at the tip region of the cantilever.

Material Properties

To simulate the Fresnel coefficients of the cantilever, the required input material property for both GaN and $Al_xGa_{1-x}N$ is their refractive index. MATLAB functions are used to provide the refractive index data of the corresponding materials to the COMSOL model. Simulations are performed within the wavelength range of 300 nm to 500 nm. For both GaN and $Al_xGa_{1-x}N$ materials, there is a real and imaginary part in their respective refractive index profiles. The real and imaginary parts of the refractive index profile are represented by n and k respectively. The refractive index profile of GaN as a function of wavelength is shown in Fig. 2 [25].

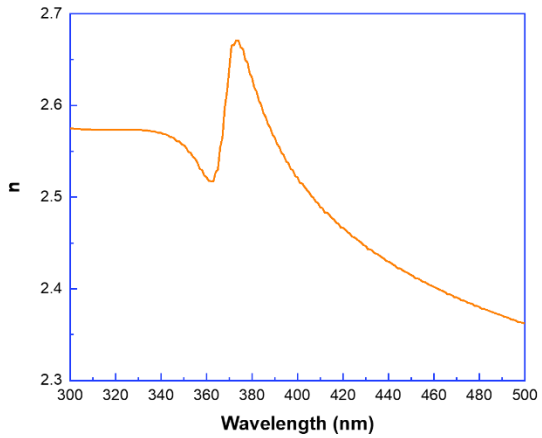

(a)

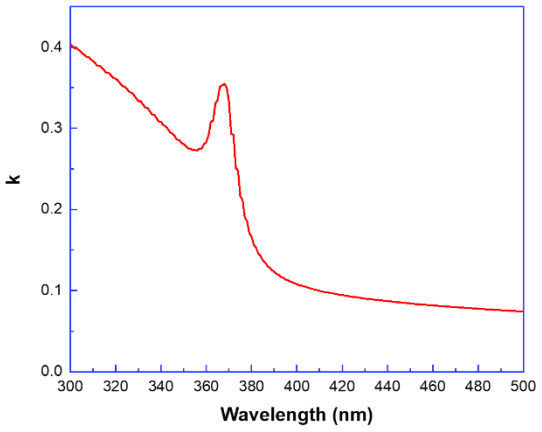

(b)

Fig. 2. (a) real, and **(b)** imaginary parts of the refractive index of GaN.

In this simulation, the Fresnel coefficients are computed for different compositions of Al in $Al_xGa_{1-x}N$. The real part of the refractive index for different Al% in $Al_xGa_{1-x}N$ is calculated by a Sellmeier type law

$$n = \sqrt{a + \frac{b \times \lambda^2}{(\lambda^2 - c^2)}}, \quad (1)$$

where n is the real part of the refractive index, λ is the wavelength, and a, b, and c are constants for a given $Al_xGa_{1-x}N$ material [26]. The a, b, and c parameters are listed in Table 1 for selected Al% values.

Table 1. Fit parameters a, b, and c of the Sellmeier law for selected Al% composition in the $Al_xGa_{1-x}N$.

Al%	a	b	c (nm)
0.19	4.98	0.39	297.7
0.47	4.20	0.63	247.5
0.675	3.95	0.63	239.3
0.785	2.67	1.67	183.7

For the given wavelength range the refractive index profile of $Al_xGa_{1-x}N$ is shown in Fig. 3.

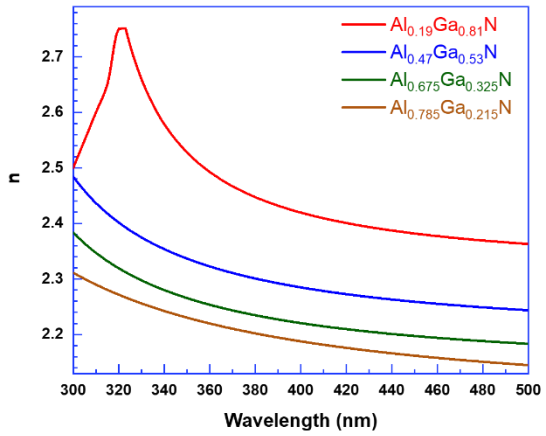

(a)

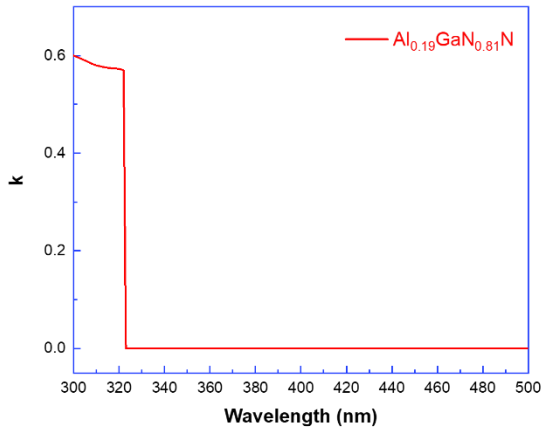

(b)

Fig. 3. (a) real, and **(b)** imaginary parts of the refractive index of $Al_xGa_{1-x}N$.

From Fig. 3 it must be noted that, except for $Al_{0.19}Ga_{0.81}N$, the imaginary part of the refractive index is 0 for the remaining Al% compositions. Also, the fit parameters of the Sellmeier law given in Table 1 for $Al_{0.19}Ga_{0.81}N$ are valid only within the wavelength range of 323 nm to 600 nm. This is because $Al_{0.19}Ga_{0.81}N$ exhibits a non-zero k value between 300 nm to 322 nm.

Governing Equations

In this model, for the given 2D geometry a linearly polarized electromagnetic wave has been launched in the $-y$ axis. It has been assumed that the electric (E) and magnetic (H) field components are along z and x axis respectively. As the H-field components are along the x axis, perfect magnetic conductor (PMC) boundary condition has been applied on both sides of the 2D geometry. Fig. 4 illustrates the 2D geometry with applied port boundary conditions. In Fig. 4, at port 1 and port 2 the wave enters and exits the cantilever respectively. Therefore, port 1 is excited with a linearly polarized electromagnetic wave having a power of 1 W.

The get the electric field distribution on the 2D geometry, the governing equation to be solved can be written as

$$\nabla \times (\nabla \times E) - k_0^2 \epsilon_r E = 0, \quad (2)$$

where $k_0 = \frac{2\pi}{\lambda}$ is the free space propagation constant and ϵ_r is the relative permittivity of the given material. For the given 2D geometry, the complex electric field E which is distributed along x and z axis can be written as

$$E(x,z) = \tilde{E}(x)e^{-jk_z z}, \quad (3)$$

where $\tilde{E}(x)$ represents the complex amplitude of the electric field distributed along the x axis and k_z is the out-of-plane wave vector component which is along the z direction. The relative permittivity of the material can be written as

$$\epsilon_r = (n - jk)^2, \quad (4)$$

where n and k are the respective real and imaginary parts of the refractive index of the material. In this simulation, the electrical conductivity (σ) and relative permeability (μ_r)of the material are assumed to be 0 and 1 respectively.

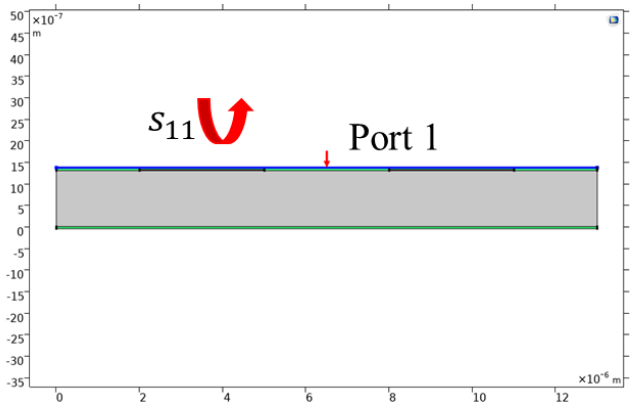

(a)

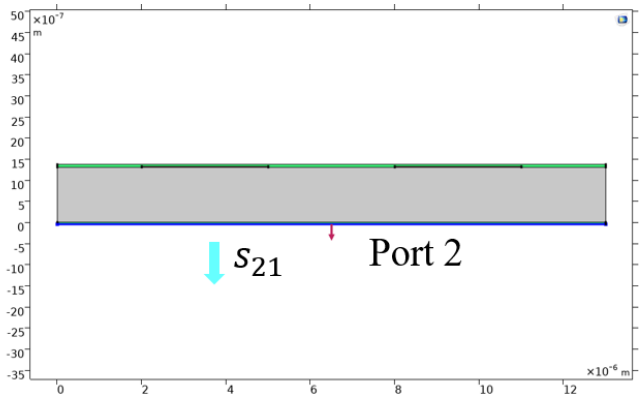

(b)

Fig. 4. 2D geometry illustrating the linearly polarized wave **(a)** enters the cantilever through port 1, and **(b)** exits through port 2.

Among the three Fresnel coefficients, the reflection (R) and transmission (T) coefficients are obtained by computing the s-parameters. The reflection and transmission coefficients are calculated as

$$R = |s_{11}|^2, \quad (5)$$

and

$$T = |s_{21}|^2 \quad (6)$$

respectively. The equation to calculate s_{11} can be written as

$$s_{11} = \frac{\iint (E_c - E_1) \cdot E_1^* \, dA_1}{\iint E_1 \cdot E_1^* \, dA_1}, \quad (7)$$

where E_c is the computed electric field, E_1 and E_1^* represent the complex and conjugate electric field at port 1. Similarly, s_{21} can be calculated as

$$s_{21} = \frac{\iint (E_c \cdot E_2^*)\, dA_2}{\iint E_2 \cdot E_2^*\, dA_2}, \quad (8)$$

where E_2 and E_2^* represent the complex and conjugate electric field at port 2. After obtaining the reflection and transmission coefficients, the absorption coefficient (A) is calculated as

$$A = 1 - R - T. \quad (9)$$

Simulation Results and Discussion

The simulations are performed for two different cases to obtain the Fresnel coefficients. In the first case the thickness of the bottom GaN layer is varied from 0.1 to 1 µm with a step size of 0.1 µm, with the Al alloy composition remaining fixed at 19%. The plots of the absorption coefficient as a function of given wavelength obtained from this study are shown in Fig. 5.

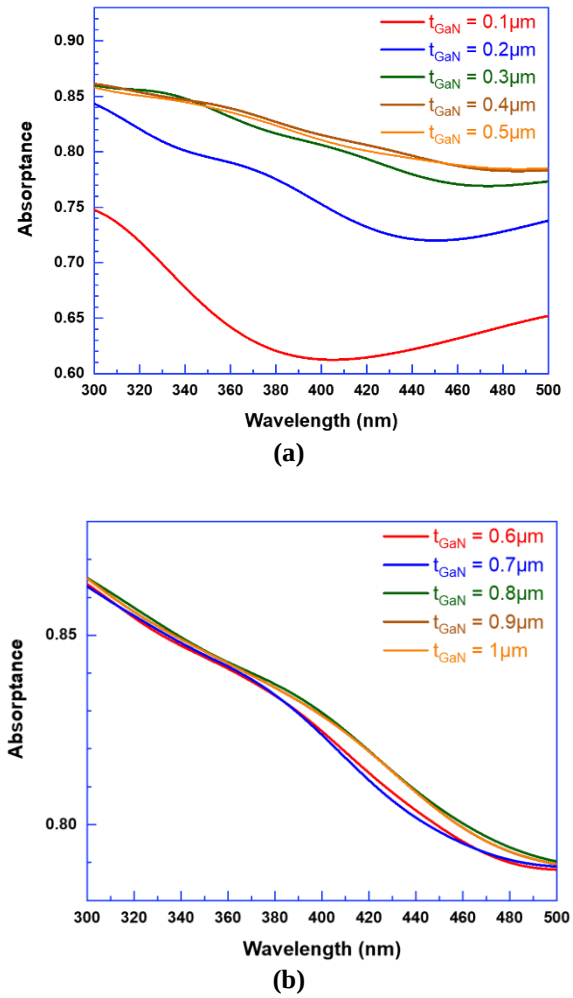

Fig. 5. Wavelength vs absorptance plots as the thickness of the bottom GaN layer varied from **(a)** 0.1 to 0.5 µm, and **(b)** 0.6 to 1 µm respectively.

From Fig. 5 it has been observed that at a wavelength of 315 nm, as the thickness of the bottom GaN layer increases from 0.1 µm to 0.5 µm, the cantilever absorptance increased monotonically from 72.82% to 85.22%. As the thickness is further increased from 0.6 µm to 1 µm, the absorption coefficient has slightly varied from 85.68% to 85.82%. Therefore, for all practical purposes from Fig. 5 it can be considered that for thicknesses > 0.5 µm, the magnitude of the absorption coefficients remains the same. The plots of the reflection coefficient as a function of given wavelength obtained for different thicknesses of the bottom GaN layer are shown in Fig. 6.

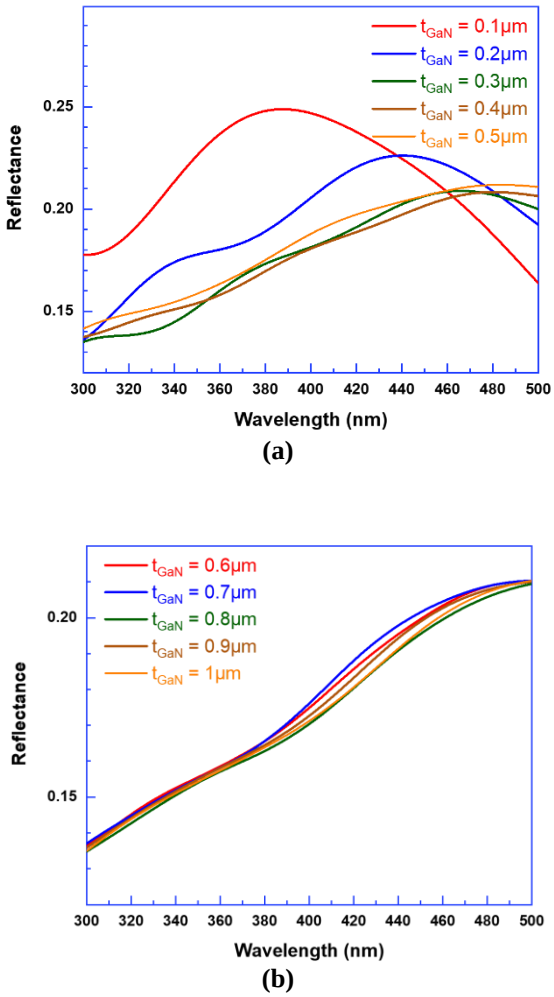

Fig. 6. Wavelength vs reflectance plots as the thickness of the bottom GaN layer varied from **(a)** 0.1 to 0.5 µm, and **(b)** 0.6 to 1 µm respectively.

From Fig. 6, it has been observed that at a wavelength of 315 nm, as the thickness increases from 0.1 µm to 0.5 µm cantilevers having bottom GaN layer thicknesses of 0.1 µm and 0.3 µm exhibits highest and lowest reflectance with a magnitude of 18.31% and 13.80% respectively. As the thickness is further increased from 0.6 µm to 1 µm, the reflectance has slightly decreased from 14.30% to 14.17%. Like the absorptance profile, for thicknesses > 0.5 µm, the magnitude of the reflection coefficients remains the same. Fig. 7 shows the plots of the transmission coefficient as a function of given wavelength for different thicknesses of the bottom GaN layer. From Fig. 7 it has been observed that at a wavelength of 315 nm, as the thickness increases from 0.1 µm to 0.5 µm, the cantilever transmittance decreased monotonically from 8.86% to 0.04%. Similarly, as the thickness is further increased from 0.6 µm to 1 µm, the transmittance is further decreased monotonically from 0.014% to 0.00014%. Therefore from Fig. 7(b), it can be concluded that at a thickness

of 1 µm, the transmittance of UV light through the proposed cantilever structure is 0. This indicates that the incident UV light is either absorbed or reflected. Also, at a thickness of 1 µm, from Fig 5 it is evident that approximately 85% of the incident photons are absorbed by the proposed cantilever respectively. For a typical UV-PD, the higher the absorptance the better is the detectivity. The absorptance can be further increased by varying the Al alloy composition in the $Al_xGa_{1-x}N$.

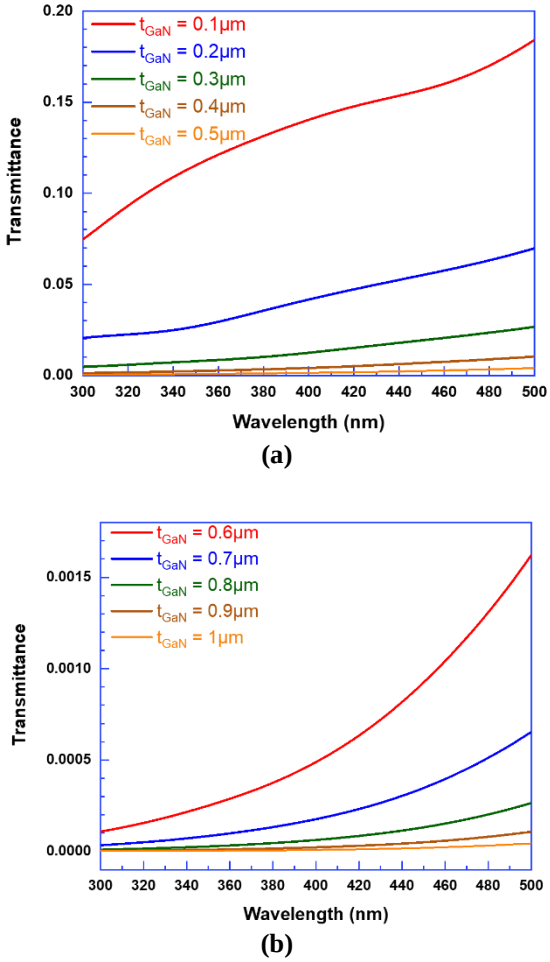

Fig. 7. Wavelength vs transmittance plots as the thickness of the bottom GaN layer varied from **(a)** 0.1 to 0.5 µm, and **(b)** 0.6 to 1 µm respectively.

In the second case, simulations are performed by varying the Al alloy composition in the $Al_xGa_{1-x}N$, with the thickness of the bottom GaN layer being fixed at 1.3 µm. In this case, the Fresnel coefficients are obtained for four different Al compositions as listed in Table 1. Fig. 8 illustrates the plot of Fresnel coefficients as a function of wavelength for different Al compositions. From Fig. 8 (a) it has been observed that at a wavelength of 315 nm, as the Al% in $Al_xGa_{1-x}N$ increases from 19% to 78.5%, the cantilever absorptance also increased monotonically from 85.80% to 90.71%. In contrast to the absorptance, in Fig. 8(b) at the wavelength of 315 nm as the Al% increases, the reflectance of the cantilever decreases monotonically from 14.20% to 9.28%. From Fig. 8(c), it is evident that irrespective of the Al alloy composition in the $Al_xGa_{1-x}N$, the transmittance of UV light through the proposed cantilever structure is 0.

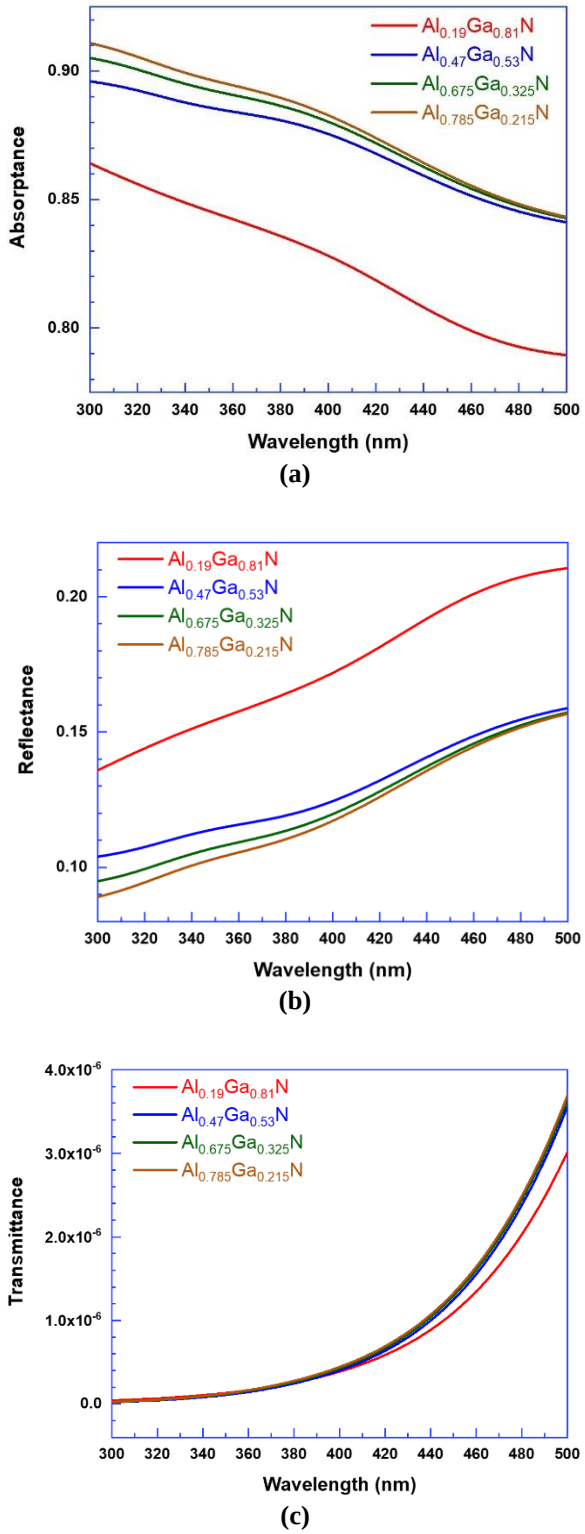

Fig. 8. Plots of **(a)** absorptance, **(b)** reflectance, and **(c)** transmittance as a function of wavelength for Al alloy compositions in $Al_xGa_{1-x}N$ respectively.

Conclusions

A novel GaN-$Al_xGa_{1-x}N$-GaN vertically stacked cantilever has been proposed to function as a UV PD. Using the wave optics module in COMSOL, the Fresnel coefficients of the cantilever are computed. With the Al alloy composition remaining fixed at 19%, the effect of bottom GaN layer thickness variation on

the Fresnel coefficients of the cantilever has been numerically studied. From the simulations, it can be concluded that for thicknesses > 0.5 μm, the absorptance and reflectance profiles remains basically unchanged. For thicknesses < 0.5 μm, the absorptance increases monotonically with the thickness of the bottom GaN layer. With the thickness of the bottom GaN layer being fixed at 1.3 μm, the effect of Al alloy composition in $Al_xGa_{1-x}N$ on the Fresnel coefficients has also been studied. From the simulation results, it can be concluded that at any given wavelength as the Al% increases, the absorptance and reflectance of the cantilever monotonically increases and decreases respectively.

In general, from the simulations it has been observed that for thicknesses ≥ 1 μm, the transmittance of UV light through the proposed cantilever is 0. The absorptance of the cantilever can be enhanced by increasing the Al alloy composition in the $Al_xGa_{1-x}N$. The numerical results obtained from this study should be useful in estimating the Fresnel coefficients which cannot be achieved experimentally.

References

1. A.Khan, K.Balalrishnan, and T.Katona, "Ultraviolet light-emitting diodes based on group three nitrides," *Nat. Photonics*, **2**, 77–84 (2008).
2. S. Zhao *et al.*, "An electrically injected AlGaN nanowire laser operating in the ultraviolet-C band," *Appl. Phys. Lett.*, **107**, 043101 (2015).
3. A. Talukdar *et al.*, "Piezotransistive transduction of femtoscale displacement for photoacoustic spectroscopy," *Nat. Comm.*, **6**, 1-10 (2015).
4. D. Khan *et al*., "Plasmonic amplification of photoacoustic waves detected using Piezotransistive GaN microcantilevers," *App. Phy. Letters.*, **111**, 062102 (2017).
5. F. Bayram *et al*., "Piezotransistive GaN microcantilevers based surface work function measurements," *Jpn. J. Appl. Phys.*, **57**, 04030 (2018).
6. M. Razeghi and A. Rogalski, "Semiconductor ultraviolet detectors," *J. Appl. Phys.*, **79**, 7433-7473 (1996).
7. L. Sang, M. Liao, Y. Koide, M. Sumiya, "High-temperature ultraviolet detection based on InGaN Schottky photodiodes," *Appl. Phys. Lett.*, **99**, 031115 (2011).
8. Y. Bie, Z. Liao, H. Zhang, G. Li, Y. Ye, Y. Zhou *et al.*, "Self-powered, ultrafast, visible-blind UV detection and optical logical operation based on Zno/GaN nanoscale P-N junctions," *Adv. Mater.*, **23**, 649-653 (2011).
9. M. Khan *et al.*, "III–Nitride UV Devices," *Jpn. J. Appl. Phys.*, **44**, 7191–7206 (2005).
10. K. H. Lee *et al.*, "AlGaN/GaN Schottky barrier UV photodetectors with a GaN sandwich layer," *IEEE Sens. J.*, **9**, 814–819 (2009).
11. T. Tut *et al.*, "Solar-blind $Al_xGa_{1-x}N$ based avalanche photodiodes," *Appl. Phys. Lett.*, **87**, 223502 (2005).
12. H. Y. Liu, Y. H. Wang, and W. C. Hsu, "Suppression of dark current on AlGaN/GaN metal-semiconductor-metal photodetectors," *IEEE Sens. J.*, **15**, 5202–5207 (2015).
13. E. Monroy, F. Calle, E. Munoz, and F. Omnes, "AlGaN metal-semiconductor-metal photodiodes," *Appl. Phys. Lett.*, **74**, 3401–3403 (1999).
14. D. B. Li *et al.*, "Effect of asymmetric Schottky barrier on GaN-based metal-semiconductor-metal ultraviolet detector," *Appl. Phys. Lett.*, **99**, 261102 (2011).
15. X. J. Sun *et al.*, "High spectral response of self-driven GaN-based detectors by controlling the contact barrier height," *Sci. Rep.*, **5**, 16819 (2015).
16. E. Monroy *et al.*, "High-quality visible-blind AlGaN p-i-n photodiodes," *Appl. Phys. Lett.*, **74**, 1171–1173 (1999).
17. D. Walker *et al.*, "Solar-blind AlGaN photodiodes with very low cutoff wavelength," *Appl. Phys. Lett.*, **76**, 403–405 (2000).
18. R. McClintock *et al.*, "High quantum efficiency AlGaN solar-blind pin photodiodes," *Appl. Phys. Lett.*, **84**, 1248–1250 (2004).
19. T. Tut, M. Gokkavas, A. Inal, and E. Ozbay, "$Al_xGa_{1-x}N$ based avalanche photo-diodes with high reproducible avalanche gain," *Appl. Phys. Lett.*, **90**, 163506 (2007).
20. L. Sun, J. L. Chen, J. F. Li, and H. Jiang, "AlGaN solar-blind avalanche photodiodes with high multiplication gain," *Appl. Phys. Lett.*, **97**, 191103 (2010).
21. Y. Huang *et al.*, "Back-illuminated separate absorption and multiplication AlGaN solar-blind avalanche photodiodes," *Appl. Phys. Lett.*, **101**, 253516 (2012).
22. M. A. Khan *et al.*, "Schottky barrier photodetector based on Mg-doped p-type GaN films," *Appl. Phys. Lett.*, **63**, 2455 (1993).
23. H. Jiang *et al.*, "Visible-blind metal-semiconductor-metal photodetectors based on undoped AlGaN/GaN high electron mobility transistor structure," *Jpn. J. Appl.Phys.*, **43**, L683 (2004).
24. E. Cicek *et al.*, "$Al_xGa_{1-x}N$ based back-illuminated solar-blind photodetectors with external quantum efficiency of 89%," *Appl. Phys. Lett.*, **103**, 191108 (2013).
25. T. Kawashima, H. Yoshikawa, and S. Adachi, "Optical properties of hexagonal GaN," *J. Appl. Phys.*, **82**, 3528 (2003).
26. N. Antoine-Vincent, *et al.*, "Determination of the refractive indices of AlN, GaN, and $Al_xGa_{1-x}N$ grown on (111) Si substrates," *J. Appl. Phys.*, **93**, 5222-5226 (2003).